Wang et al. Nanoscale Research Letters (2018) 13:33
DOI 10.1186/s11671-018-2448-y

Nanoscale Research Letters

NANO IDEA Open Access

PtNi Alloy Cocatalyst Modification of Eosin Y-Sensitized g-C_3N_4/GO Hybrid for Efficient Visible-Light Photocatalytic Hydrogen Evolution

Peng Wang, Lanlan Zong, Zhongjie Guan*, Qiuye Li* and Jianjun Yang

Abstract

An economic and effective Pt-based alloy cocatalyst has attracted considerable attention due to their excellent catalytic activity and reducing Pt usage. In this study, PtNi alloy cocatalyst was successfully decorated on the g-C_3N_4/GO hybrid photocatalyst via a facile chemical reduction method. The Eosin Y-sensitized g-C_3N_4/PtNi/GO-0.5% composite photocatalyst yields about 1.54 and 1178 times higher hydrogen evolution rate than the Eosin Y-sensitized g-C_3N_4/Pt/GO-0.5% and g-C_3N_4/Ni/GO-0.5% samples, respectively. Mechanism of enhanced performance for the g-C_3N_4/PtNi/GO composite was also investigated by different characterization, such as photoluminescence, transient photocurrent response, and TEM. These results indicated that enhanced charge separation efficiency and more reactive sites are responsible for the improved hydrogen evolution performance due to the positive synergetic effect between Pt and Ni. This study suggests that PtNi alloy can be used as an economic and effective cocatalyst for hydrogen evolution reaction.

Keywords: PtNi alloy cocatalyst, g-C_3N_4/GO, Eosin Y-sensitization, Hydrogen evolution

Background

Sustainable and large-scale hydrogen evolution from water using solar energy is considered to be one of the promising method toward solving the energy crisis and environmental pollution [1, 2]. To achieve this goal, a visible-light response photocatalyst and an efficient cocatalyst are required [3–5]. Usually, loading noble metal Pt as an efficient cocatalyst is highly necessary for achieving a high hydrogen evolution rate [6–8]. However, Pt is rare and expensive, which hinders its practical application. Reducing the amount of Pt usage while simultaneously maintaining its excellent catalytic activity for hydrogen evolution is desired. Replacing part of Pt with transition metal (Ni, Co, Cu, Fe, etc.) to form a bimetallic alloy cocatalyst is a promising potential way for achieving excellent catalytic activity and reducing the use of Pt [9–11]. In some case, the catalytic performance of Pt-based bimetallic alloy cocatalyst is comparable with pure Pt due to the positive synergetic effect between the two metals. Therefore, a visible-light response photocatalyst loaded with a bimetallic alloy cocatalyst has been paid more attention in recently.

Yu et al. reported that PtCo or PtNi alloy cocatalyst-modified Cu_2ZnSnS_4 showed higher H_2 production efficiency than the pure Pt loading Cu_2ZnSnS_4 [12]. Pt_3Co bimetallic cocatalyst decorated CdS were prepared by Hu et al. and exhibited enhanced hydrogen evolution performance [13]. PtCo and/or PtFe loading $Zn_{1-x}Cd_xS$ were also evaluated in previous studies [14, 15]. However, low visible-light photocatalytic performance of Cu_2ZnSnS_4 or high toxicity of Cd hinders their practical application on a large scale. Carbon nitride (g-C_3N_4) has attracted attention due to its low cost [16]. Han et al. reported that a H_2 evolution rate of 960 μmol g^{-1} h^{-1} was obtained over the PtCo/g-C_3N_4 photocatalyst under $\lambda > 400$ nm irradiation [17]. $PtNi_x$/g-C_3N_4 hybird photocatalyst was also studied by Bi et al., and a H_2 evolution rate of 8456 μmol g^{-1} h^{-1} was achieved under full spectral irradiation [18]. However, the visible-light photocatalytic

* Correspondence: guanzj@henu.edu.cn; qiuyeli@henu.edu.cn
National & Local Joint Engineering Research Center for Applied Technology of Hybrid Nanomaterials, Henan University, Kaifeng 475004, China

performance for the bimetallic alloy cocatalyst-modified g-C_3N_4 photocatalyst is still a little bit low due to the wide band gap of 2.7 eV and bad electron transfer ability. Eosin Y-sensitized g-C_3N_4 can harvest a wide range of visible light [19, 20]. Graphene oxide (GO) possesses highly electron transporting property and has been widely used as an electron acceptor [21–25]. Combining g-C_3N_4 and GO can promote the electron transfer capability in g-C_3N_4 and thus improve the electron-hole pair's separation to improve the photocatalytic performance for hydrogen evolution [26–31]. Lately, we reported an efficient Eosin Y-sensitized g-C_3N_4/Pt/GO composite photocatalyst for hydrogen evolution [23]. The expensive Pt cocatalyst plays one of the important role for the relatively high hydrogen production performance. In order to decrease the expensive Pt usage and further improve its visible photocatalytic performance, exploiting low-cost Eosin Y-sensitized g-C_3N_4/GO composite photocatalyst loaded with Pt-based alloy cocatalyst is useful.

Here, the Eosin Y-sensitized g-C_3N_4/PtNi/GO composite photocatalyst was prepared for hydrogen evolution from water. The highest hydrogen evolution rate of 5.89 mmol g^{-1} h^{-1} is obtained over the Eosin Y-sensitized g-C_3N_4/PtNi/GO photocatalyst, which is much higher than the Eosin Y-sensitized g-C_3N_4/Pt/GO and g-C_3N_4/Ni/GO composite samples. To the best our knowledge, there is no previous report that the Eosin Y-sensitized g-C_3N_4/PtNi/GO composite is employed for hydrogen production from water. The optimal molar ratio of Pt/Ni and amount of PtNi cocatalyst were screened out in detail. In addition, mechanism of enhanced photocatalystic performance for the g-C_3N_4/PtNi/GO composite was also investigated through different characterization methods.

Experimental Section

Synthesis of the g-C_3N_4

g-C_3N_4 powders were synthesized as described in previous study [32]. In a typical procedure, urea (8 g) was placed in an alumina crucible with a cover. The crucible was heated to 600 °C at a heating rate of 5 °C/min and held for 2 h in a tube furnace. After thermal treatment, the light yellow g-C_3N_4 powders were collected for further using.

Preparation of GO

GO was prepared using the modified Hummers' method [33]. Nature graphite (10 g) and $NaNO_3$ (5 g) were putted into a beaker. Then, 230 mL concentrated sulfuric acid were added, and the process must be as slow as possible. The above reaction was proceeded with stirring under ice-water bath. Next, 10 g $KMnO_4$ was added into the mixture solution and reacted for 3 h. The temperature of solution was raised to 35 °C and was maintained for 4 h. Then, 460-mL distilled water was poured into the above solution and heated up to about 98 °C for 3 h. After reaction, a certain amount of H_2O_2 (30%) and concentrated hydrochloric acid were added under stirring with the purpose of removing excess $KMnO_4$ and SO_4^{2-}. Finally, the GO sample was obtained by freeze-drying for 24 h.

Synthesis of g-C_3N_4/Ni/GO, g-C_3N_4/Pt/GO, and g-C_3N_4/Pt_xNi_y/GO Composite Photocatalysts

Synthesis of g-C_3N_4/PtNi/GO-*X* (*X* represents the weight ratio of PtNi cocatalyst to g-C_3N_4/GO composite and the molar ratio of Pt to Ni is 1:1): In a typical, 133 mg of g-C_3N_4 were dispersed into 50 mL anhydrous ethanol. Excess $NaBH_4$ reductant was added into the mixture solution under stirring. Then, a certain volume of $NiCl_2{\cdot}6H_2O$ solution (0.1 mol/L) and H_2PtCl_6 solution (1.0 mmol/L) were dropwise added into the above solution. In order to investigate the added procedure of $NiCl_2{\cdot}6H_2O$ and H_2PtCl_6 solutions, three methods including simultaneous loading of Pt and Ni, loading of Pt and then Ni or in reverse were chose. Then, the suspension solution was stirred for 5 h to achieve a uniform dispersion for PtNi cocatalyst in the g-C_3N_4. After that, the g-C_3N_4/PtNi-X samples were collected by centrifugation to wash away excess $NaBH_4$ for several times. Afterwards, 67 mg GO and the g-C_3N_4/PtNi-X sample were dispersed into 100-mL distilled water simultaneously. The suspension solution was ultrasonicated at 500 W for 10 h. After that, a series of g-C_3N_4/PtNi/GO-*X* composite photocatalysts were obtained by centrifuged and then dried at 60 °C in a vacuum oven for one night. Other bimetallic PtNi alloy cocatalysts with different Pt/Ni molar ratio (9:1, 3:1, 1:3, 1:9) were also prepared as same as the aforementioned method, which named as Pt_9Ni_1, Pt_3Ni_1, Pt_1Ni_3, and Pt_1Ni_9, respectively, specially, the 1:1 M ratio of Pt/Ni name as PtNi.

Synthesis of g-C_3N_4/Ni/GO-0.5% and g-C_3N_4/Pt/GO-0.5% samples (0.5% represents the weight ratio of Ni or Pt to the g-C_3N_4/GO composite): The g-C_3N_4/Ni/GO-0.5% and g-C_3N_4/Pt/GO-0.5% samples were prepared with the same preparation procedure of g-C_3N_4/PtNi/GO-X samples except for adding different volume of $NiCl_2{\cdot}6H_2O$ solution or H_2PtCl_6 solution. The 2:1 weight ratio of g-C_3N_4 to GO is chosen in all g-C_3N_4/Ni/GO, g-C_3N_4/Pt/GO, and g-C_3N_4/Pt_xNi_y/GO composite samples according to our previous study [32].

Characterization Methods

The XRD patterns were obtained using an X-ray diffraction diffractometer (Bruker D8-Advance, Germany) with Cu-Kα radiation. TEM images of the samples were recorded through the transmission electron microscopy (JEM-2100, Japan). Surface chemical states of the photocatalysts were measured by X-ray photo-electron

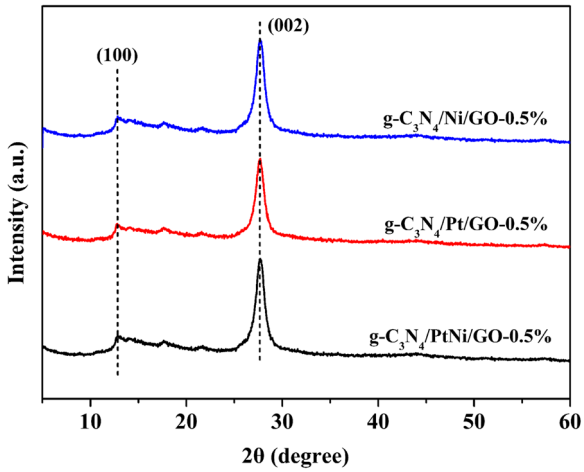

Fig. 1 The XRD patterns of g-C_3N_4/Ni/GO-0.5%, g-C_3N_4/Pt/GO-0.5%, and g-C_3N_4/PtNi/GO-0.5% samples

spectroscopy (XPS, AXISULTRA) with monochromatic Al Ka X-rays (1486.6 eV). The photoluminescence (PL) spectra were measured on a JY HORIBA FluoroLog-3 spectrometer, and the excited wavelength of 460 nm was chosen. The curves of photocurrent response were carried out in an electrochemical workstation (CHI660E, Chenhua, China) using a conventional standard three-electrode cell under visible light irradiation ($\lambda > 420$ nm). 0.1 mol/L Na_2SO_4 solution was used as electrolyte.

Photocatalytic Activity Measurement

Photocatalytic experiments were conducted in a Pyrex cell with a top flat window at 6 °C. Typically, 50 mg photocatalyst powder and 50 mg Eosin Y dye were added into 100 mL H_2O containing 20 vol% (*v*/v) triethanolamine (TEOA, pH = 7). A 300-W xenon lamp (D59, Beijing China Education Au-light Co., Ltd) coupled with a UV cut-off filter (> 420 nm) was used as the light source. The amounts of hydrogen were measured through a gas chromatography (GC-7920, TCD, Ar carrier).

Results and Discussion

The XRD patterns of g-C_3N_4/Ni/GO-0.5%, g-C_3N_4/Pt/GO-0.5%, and g-C_3N_4/PtNi/GO-0.5% samples are shown in Fig. 1. Two obvious diffraction peaks are observed for the three samples. A small peak centered at $2\theta = 13.8°$ is assigned to the (100) peak of g-C_3N_4, which arises from the in-plane structural packing motif [34]. The strong diffraction peak at 27.4° is indexed as the (002) peak of g-C_3N_4, which corresponds to the interlayer stacking of conjugated aromatic system [35]. For the three evaluated samples, no GO, Pt and/or Ni cocatalyst diffraction signal were detected. Sufficient exfoliation of GO in the composite can result in no GO information [28]. While the amount of Pt and/or Ni are too small to detect by XRD method. As shown in Fig. 2, the three different samples exhibit similar thinner laminar structure after ultrasonic treatment. An intimate contact formed between 2D-layered structure of g-C_3N_4 and the nanosheet structure of GO. In Fig. 2a, b, a bit larger of Ni or Pt nanoparticles are dispersed on the interlayer or surface of g-C_3N_4. Compared with pure Ni and Pt, the size of the PtNi alloy cocatalyst particles is reduced and the dispersion of PtNi alloy cocatalyst is improved (see Fig. 2c). The small size of PtNi alloy cocatalyst will provide more reactive sites for hydrogen evolution, and the high dispersion of PtNi alloy cocatalyst is benefited to the electrons transfer from g-C_3N_4 and/or GO to PtNi cocatalyst. The improved dispersion of PtNi alloy cocatalyst was also observed in previous study [36]. The precision reason need further investigate.

In order to investigate the surface chemical element and valence states of g-C_3N_4/Ni/GO, g-C_3N_4/Pt/GO, and g-C_3N_4/PtNi/GO samples, high-resolution XPS spectra of the three different samples were measured and the results are shown in Fig. 3. In Fig. 3a, the XPS spectrum of C 1 s can be fitted into two strong peaks with the binding energies at about 284.8 eV and

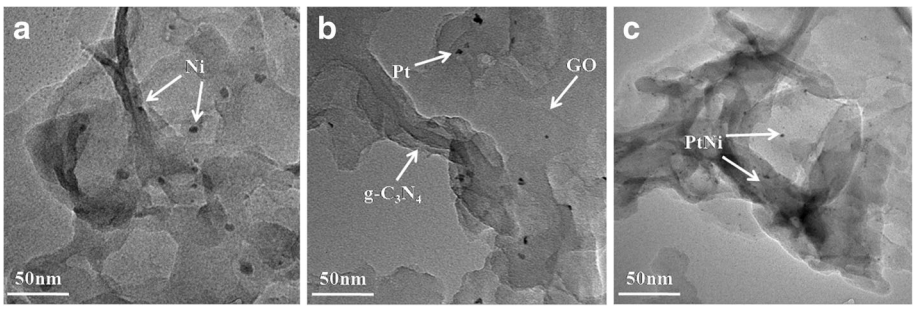

Fig. 2 TEM images of g-C_3N_4/Ni/GO-0.5% (**a**), g-C_3N_4/Pt/GO-0.5% (**b**), and g-C_3N_4/PtNi/GO-0.5% (**c**)

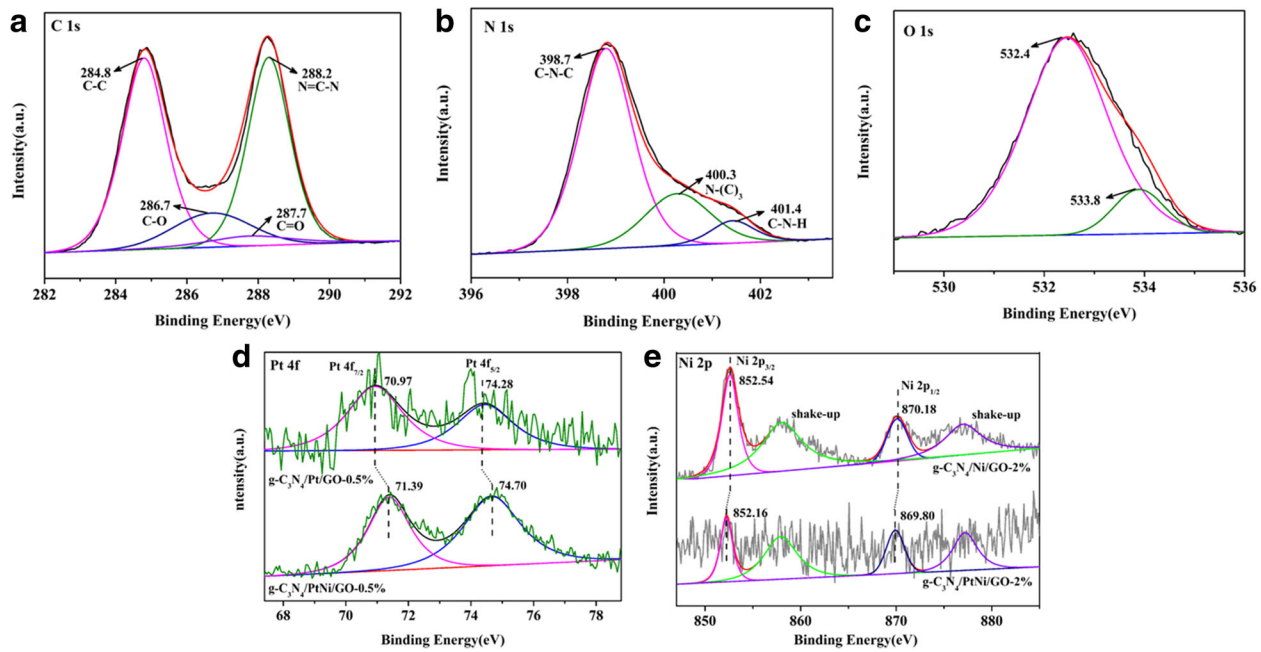

Fig. 3 XPS spectra of (**a**) C 1 s, (**b**) N 1 s and (**c**) O 1 s for the g-C_3N_4/PtNi/GO-0.5% sample. **d** XPS spectra of Pt 4f for the g-C_3N_4/Pt/GO-0.5% and g-C_3N_4/PtNi/GO-0.5% samples. **e** XPS spectra of Ni 2p for the g-C_3N_4/Ni/GO-2% and g-C_3N_4/PtNi/GO-2% samples

288.2 eV, which are assigned to C-C and N=C-N, respectively [37]. The two peaks are the characteristic of carbon species in g-C_3N_4. Two small peaks at 286.7 eV and 287.7 eV are also obtained, which belong to the C-O and C=O functional groups on the surface of GO, respectively [38]. In Fig. 3 (b), the characteristic peaks of C-N-C, N-$(C)_3$, and C-N-H groups in g-C_3N_4 were detected, which are located at the binding energies of 398.7, 400.3, and 401.4 eV, respectively [39]. In Fig. 3 (c), the banding energies of O 1 s are found at 532.4 and 533.8 eV, which are assigned to oxygen-containing functional groups in the composite sample and surface adsorption of oxygen species, respectively [40]. Figure 3 (d) exhibits the XPS spectra of the Pt 4f doublet ($4f_{7/2}$ and $4f_{5/2}$). The Pt $4f_{7/2}$ and $4f_{5/2}$ peaks are located at 70.97 and 74.28 eV for the g-C_3N_4/Pt/GO-0.5% sample, respectively, which represent the signal of Pt^0 [41, 42]. For the g-C_3N_4/PtNi/GO-0.5% sample, the orbital binding energies of Pt 4f shift about 0.42 eV to high binding energy compared with pure Pt. The obvious peak shift suggests that Pt electron is slight loss, which indicates that the PtNi alloy cocatalyst is formed in the g-C_3N_4/PtNi/GO-0.5% sample. As shown in Fig. 3e, the binding energies at 852.54 and 870.18 eV can be assigned to Ni $2p_{3/2}$ and Ni $2p_{1/2}$ for the g-C_3N_4/Ni/GO-2% sample, respectively, which are the characterization signal of Ni^0 [43]. Compared with g-C_3N_4/Ni/GO-2%, the binding energies of Ni 2p shifted to low binding energy for the g-C_3N_4/PtNi/GO-2% sample. The result suggests that a change in the surrounding environment of Ni atoms occurs, which further confirms that the PtNi alloy cocatalyst is successfully synthesized [41]. The exact molar ratio of Pt to Ni in the g-C_3N_4/PtNi/GO-0.5% sample is 9:11 through XPS measurement. Based on above analysis, it can be concluded that the g-C_3N_4/PtNi/GO composite with PtNi alloy as cocatalyst was obtained by combing a facile liquid-phase sonochemical way with a chemical reduction method.

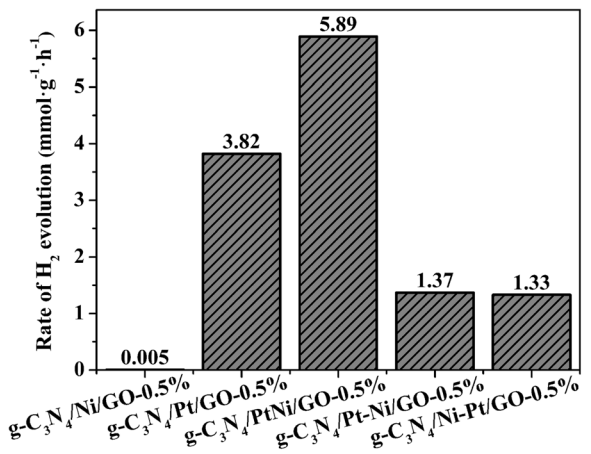

Fig. 4 H_2 evolution rate of series of g-C_3N_4/PtNi/GO-0.5% samples loaded with different type of cocatalyst. Light source: 300 W Xenon lamp ($\lambda > 420$ nm). Reaction solution: 100 mL 20% (*v*/*v*) TEOA aqueous solution (pH = 7)

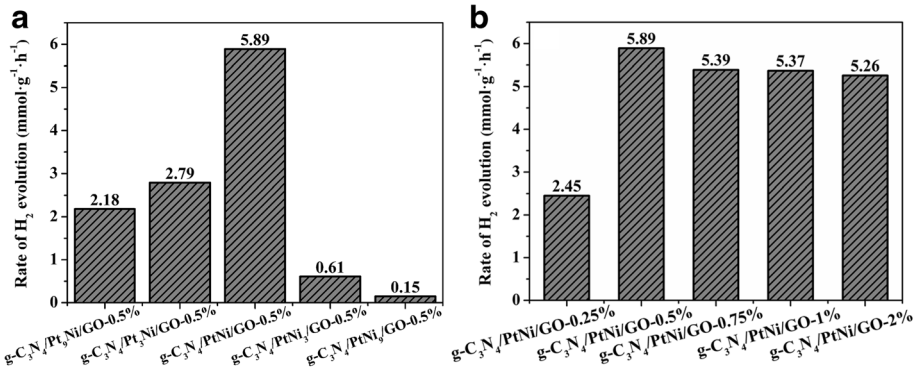

Fig. 5 **a** H_2 production rate of g-C_3N_4/Pt_xNi_y/GO-0.5% samples loaded with different Pt/Ni molar ratio. **b** H_2 production rate of g-C_3N_4/PtNi/GO samples loaded with different amounts of PtNi alloy cocatalyst. Light source: 300 W Xenon lamp (λ > 420 nm). Reaction solution: 100 mL 20% (*v*/*v*) TEOA aqueous solution (pH = 7)

Figure 4 shows the H_2 evolution rate of series of g-C_3N_4/PtNi/GO-0.5% samples loaded with different type of cocatalyst. Simultaneous loading of Pt and Ni names as g-C_3N_4/PtNi/GO-0.5%; Loading of Pt and then Ni names as g-C_3N_4/Pt-Ni/GO-0.5%; Loading of Ni and then Pt names as g-C_3N_4/Ni-Pt/GO-0.5%. For Eosin Y-sensitized g-C_3N_4/Ni/GO-0.5% sample with pure Ni as cocatalyst, the H_2 evolution rate is very low and only reach to 0.005 mmol g^{-1} h^{-1}. After replacing Ni with Pt as cocatalyst, a significant increase of H_2 evolution rate is observed, which sharply increases to 3.82 mmol g^{-1} h^{-1} for the Eosin Y-sensitized g-C_3N_4/Pt/GO-0.5% sample. The result suggests that loading efficient Pt cocatalyst is necessary to achieve excellent performance for H_2 generation. When employed PtNi alloy as cocatalyst, the Eosin Y-sensitized g-C_3N_4/PtNi/GO-0.5% composite shows the highest H_2 evolution rate of 5.89 mmol g^{-1} h^{-1}, which is about 1.54 and 1178 times higher than the Eosin Y-sensitized g-C_3N_4/Pt/GO-0.5% and g-C_3N_4/Ni/GO-0.5% samples, respectively. The enhanced performance can be attributed to the positive synergistic effect between Pt and Ni. Compared with pure Pt cocatalyst, PtNi alloy cocatalyst accelerates the accumulation of photongenerated electrons, which will provide more electrons for hydrogen evolution [18]. In addition, the small size and high dispersion of PtNi alloy cocatalyst can provide more H_2 evolution sites and enhance the electrons transfer, respectively. When loaded Pt and then Ni or in reverse, an obvious reduction of H_2 evolution activity is observed. In fact, loading Pt and then Ni or in reverse does not form PtNi alloy cocatalyst [44]. The result indicates that achieving high H_2 generation rate is strongly relied on employing efficient PtNi alloy cocatalyst.

The composition of PtNi alloy cocatalyst has an important effect on the catalytic activity for H_2 evolution. Therefore, the H_2 production rate of Eosin Y-sensitized g-C_3N_4/Pt_xNi_y/GO-0.5% samples loaded with different Pt/Ni molar ratio were investigated and the results are shown in Fig. 5a. The H_2 production rate is increased gradually with increasing Ni/Pt molar ratio. When the molar ratio of Ni/Pt is 1:1, the highest hydrogen production rate of 5.89 mmol g^{-1} h^{-1} is obtained. Further increasing the amount of Ni leads to a drop in the H_2 evolution activity. The degradation of H_2 generation performance may come from the reducing number of Pt active sites for H_2 evolution. Pt active sites have stronger adsorption of hydrogen ions than Ni [12]. Therefore, H_2 evolution preferentially takes places on Pt instead of Ni. Figure 5b shows the H_2 production rate of Eosin Y-sensitized g-C_3N_4/PtNi/GO samples loaded with different amounts of PtNi alloy cocatalyst. When the weight

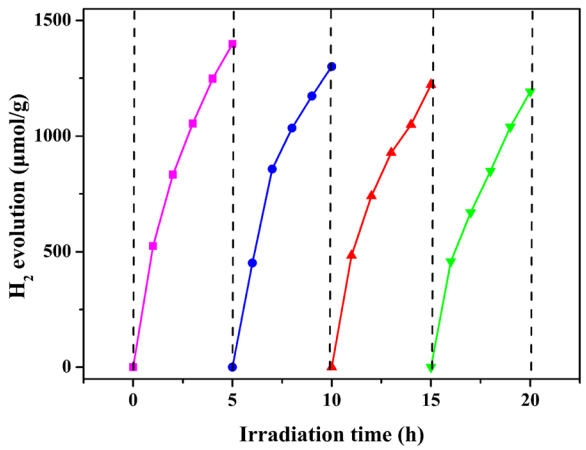

Fig. 6 Cyclic H_2 production for the g-C_3N_4/PtNi/GO-0.5% sample. Light source: 300 W Xenon lamp (λ > 420 nm), Reaction solution: 100 mL 20% (v/v) TEOA aqueous solution (pH = 7), photocatalyst, 50 mg, the weight ratio of Eosin Y to Photocatalyst is 1:1

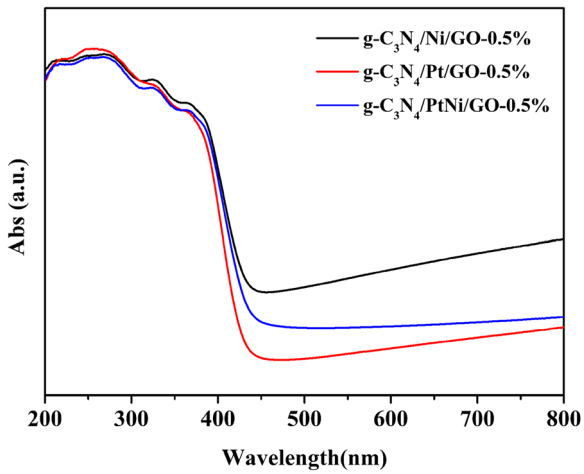

Fig. 7 UV-Vis diffuse reflectance spectra of g-C_3N_4/Ni/GO-0.5%, g-C_3N_4/Pt/GO-0.5%, and g-C_3N_4/PtNi/GO-0.5% samples

content of PtNi alloy cocatalyst is 0.5%, a hydrogen evolution rate of 2.45 mmol g^{-1} h^{-1} is obtained for the g-C_3N_4/PtNi/GO-0.25% sample. The hydrogen evolution rate increases from 2.45 mmol g^{-1} h^{-1} to the highest value of 5.89 mmol g^{-1} h^{-1} after the amount of PtNi alloy cocatalyst up to 0.5%. In further increasing the amount of PtNi alloy cocatalyst, the hydrogen evolution performance shows a slight decrease. Excess PtNi alloy cocatalyst can hinder the light absorption of Eosin Y and g-C_3N_4 and thus degrade the photocatalytic performance. The stability of hydrogen generation for the g-C_3N_4/PtNi/GO-0.5% sample was also measured and the result is shown in Fig. 6. After 4 cycle test, the hydrogen generation rate for the g-C_3N_4/PtNi/GO-0.5% sample shows a slight decrease, which indicates that the g-C_3N_4/PtNi/GO-0.5% composite sample has relatively stability for hydrogen evolution. A strong covalent bond between the carbon and nitride in C_3N_4 and the weak degradation of Eosin Y are the two main reasons for the hydrogen evolution stability of g-C_3N_4/PtNi/GO-0.5% sample [19, 45].

In order investigate mechanism for the improved photocatalystic performance of g-C_3N_4/PtNi/GO sample with PtNi alloy as cocatalyst, two possible reasons of light absorption and charge separation efficiency were evaluated. Figure 7 shows the UV-Vis diffuse reflectance spectra of g-C_3N_4/Ni/GO-0.5%, g-C_3N_4/Pt/GO-0.5%, and g-C_3N_4/PtNi/GO-0.5% samples. The three different samples exhibit an obvious absorption after about 450 nm, which is from the metal cocatalyst [18]. The g-C_3N_4/Ni/GO-0.5% sample with pure Ni as cocatalyst shows the strongest absorption after about 450 nm. However, the H_2 evolution rate for the g-C_3N_4/Ni/GO-0.5% sample is the lowest. The result suggests that the improved H_2 evolution performance is not coming from the enhanced light absorption.

Charge separation efficiency can be characterized by the photoluminescence (PL) quenching spectra [46, 47]. In general, a strong intensity of PL spectra indicates serious charge carrier recombination. Figure 8a shows the photoluminescence (PL) quenching spectra of Eosin Y by the g-C_3N_4/Ni/GO-0.5%, g-C_3N_4/Pt/GO-0.5%, and g-C_3N_4/PtNi/GO-0.5% samples. Only the Eosin Y solution without photocatalyst exhibits an extensive emission peak at about 540 nm because of Eosin Y's conjugate xanthene structure and strong recombination capacity of photogenerated electron-hole pairs in excited Eosin Y. Obvious fluorescence quenching is observed after adding different type of photocatalysts into the Eosin Y solution. The fluorescence quenching suggests that the electrons transfer to photocatalysts from excited Eosin Y and then migrate to cocatalyst for proton reduction. In addition, there is a small blue shift (ca. 1.3 nm) of PL quenching

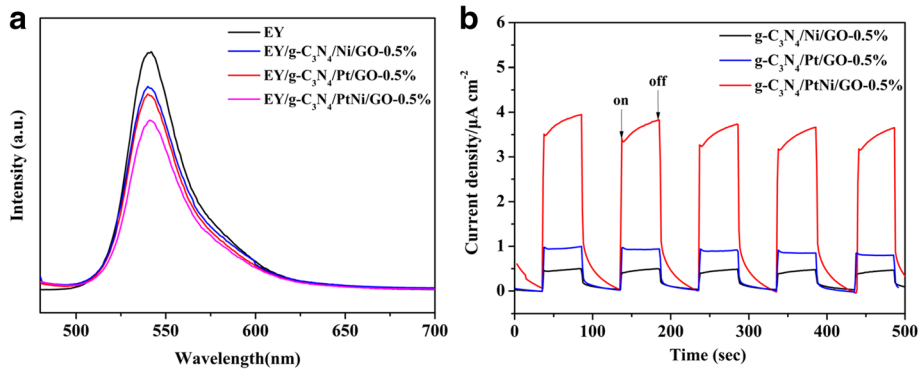

Fig. 8 a The photoluminescence (PL) quenching spectra by g-C_3N_4/Ni/GO-0.5%, g-C_3N_4/Pt/GO-0.5% and g-C_3N_4/PtNi/GO-0.5% samples in 20% (v/v) TEOA aqueous solution (pH = 7). Eosin Y solution: 0.01 mM (**b**) Transient photocurrent responses of g-C_3N_4/Ni/GO-0.5%, g-C_3N_4/Pt/GO-0.5% and g-C_3N_4/PtNi/GO-0.5% samples

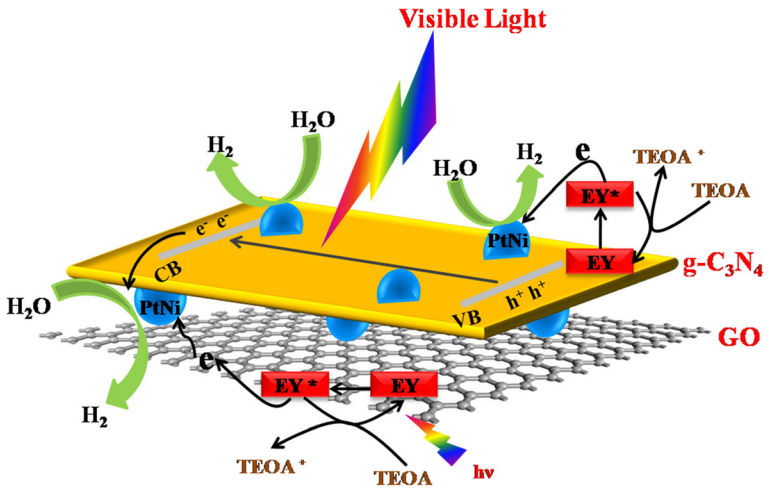

Fig. 9 A schematic diagram of H_2 evolution process for the Eosin Y-sensitized g-C_3N_4/PtNi/GO composite sample under visible light irradiation

spectra for the three different evaluated composite photocatalysts, which can be attributed to the noncovalent π-π stacking interaction among Eosin Y, g-C_3N_4 and GO [48]. The PL quenching spectra of g-C_3N_4/Pt/GO-0.5% sample shows a moderated intensity, which is lower than the g-C_3N_4/Ni/GO-0.5% sample. Importantly, the g-C_3N_4/PtNi/GO-0.5% sample exhibits the lowest fluorescence intensity, which implies that the PtNi alloy cocatalyst is the most efficient cocatalyst for improving the charge separation efficiency than pure Pt or Ni. The result is consistent with the H2 evolution activity (see Fig. 4). To further verify the charge transfer process, the transient photocurrent responses of g-C_3N_4/Ni/GO-0.5%, g-C_3N_4/Pt/GO-0.5%, and g-C_3N_4/PtNi/GO-0.5% samples were measured and the results are shown in Fig. 8b. The g-C_3N_4/PtNi/GO-0.5% sample exhibits the highest photocurrent response under visible-light irradiation ($\lambda > 420$ nm), which further confirms employing PtNi alloy cocatalyst is essential to improve charge separation efficiency. Based on above results, the improved H2 evolution activity for the Eosin Y-sensitized g-C_3N_4/PtNi/GO-0.5% composite is attributed to the enhanced charge separation efficiency.

According to above results and mechanism analysis, we propose a schematic diagram to understand the H_2 evolution process for the Eosin Y-sensitized g-C_3N_4/PtNi/GO composite sample (Fig. 9). Under visible-light irradiation, the photogenerated electrons in the LUMO of excited Eosin Y transfer to g-C_3N_4 and/or GO and then to the PtNi alloy cocatalyst for protons reduction. Meanwhile, the photoexcited electrons in the CB of g-C_3N_4 also flow to the PtNi alloy cocatalyst for H_2 evolution reaction. At the same time, the photogenerated holes or oxidized Eosin Y dyes directly oxide the TEOA sacrificial agent.

Conclusion

Ternary g-C_3N_4/PtNi/GO composite was synthesized by combing a facile liquid-phase sonochemical way with a chemical reduction method. The Eosin Y-sensitized g-C_3N_4/PtNi/GO-0.5% composite shows the highest hydrogen evolution rate of 5.89 mmol g^{-1} h^{-1}, which is about 1.54 and 1178 times higher than the Eosin Y-sensitized g-C_3N_4/Pt/GO-0.5% and g-C_3N_4/Ni/GO-0.5% samples, respectively. The enhanced photocatalytic activity can be ascribed to the positive synergetic effect between Pt and Ni as well as more reactive sites, which leads to efficient photoexcited electron-hole pairs separation. This study demonstrates that PtNi alloy can be employed as an economic and efficient cocatalyst for photocatalytic hydrogen evolution.

Acknowledgements

The authors gratefully acknowledge financial support from the National Natural Science Foundation of China (51702087, 21673066, and 21703054), Program for Science & Technology Innovation Talents (15HASTIT043) and Innovative Research Team (16IRTSTHN015) from the University of Henan Province.

Authors' Contributions

This manuscript was written by PW. The preparation and characterization of samples were conducted by PW. The analysis and discussion of the results are carried out by PW, ZG, QL, LZ, JY. All authors revised and approved the final manuscript.

Competing Interests

The authors declare that they have no competing interests.

Publisher's Note

Received: 28 December 2017 Accepted: 21 January 2018
Published online: 02 February 2018

References

1. Fujishima A, Honda K (1972) Electrochemical photolysis of water at a semiconductor electrode. Nature 238:37–38
2. Wang X, Maeda K, Thomas A, Takanabe K, Xin G, Carlsson J, Domen K, Antonietti M (2009) A metal-free polymeric photocatalyst for hydrogen production from water under visible light. Nat Mater 8:76–80
3. Hou Y, Laursen A, Zhang J, Zhang G, Zhu Y, Wang X, Dahl S, Chorkendorff I (2013) Layered nanojunctions for hydrogen-evolution catalysis. Angew Chem Int Ed 52:3621–3625
4. Jin Z, Yang H (2013) Exploration of Zr-metal-organic framework as efficient photocatalyst for hydrogen production. Nanoscale Res Lett 12:539–549
5. Yuan Y, Chen D, Zhong J, Yang L, Wang J, Liu M, Tu W, Yu Z, Zou Z (2017) Interface engineering of a noble-metal-free 2D–2D MoS_2/Cu-$ZnIn_2S_4$ photocatalyst for enhanced photocatalytic H2 production. J Mater Chem A 5:15771–15779
6. Li X, Yu J, Low J, Fang Y, Xiao J, Chen X (2015) Engineering heterogeneous semiconductors for solar water splitting. J Mater Chem A 3:2485–2534
7. Zhang X, Peng T, Song S (2016) Recent advances in dye-sensitized semiconductor systems for photocatalytic hydrogen production. J Mater Chem A 4:2365–2402
8. Li Y, Wang L, Liang J, Gao F, Yin K, Dai P (2017) Hierarchical heterostructure of ZnO@TiO_2 hollow spheres for highly efficient photocatalytic hydrogen evolution. Nanoscale Res Lett 12:531–536
9. Takako H, Hiroyuki U, Masahiro W (1999) Enhancement of the electroreduction of oxygen on Pt alloys with Fe, Ni, and Co. J Electrochem Soc 146:3750–3756
10. Garciacontreras M, Fernandezvalverde S, Vargasgarcia J, Cortesjacome M, Toledoantonio J, Angeleschavez C (2008) Pt, PtCo and PtNi electrocatalysts prepared by mechanical alloying for the oxygen reduction reaction in 0.5M H_2SO_4. Int J Hydrog Energy 33:6672–6680
11. Qin L, Li X, Kang S (2013) Synergetic effect of Cu-Pt bimetallic co-catalyst on $SrTiO_3$ for efficient photocatalytic hydrogen production from water. RSC Adv 00:1–3
12. Yu X, An X, Genç A, Ibáñez M, Arbiol J, Zhang Y, Cabot A (2015) Cu_2ZnSnS_4–PtM (M = Co, Ni) Nanoheterostructures for Photocatalytic Hydrogen Evolution. J Phys Chem C 119:21882–21888
13. Hu Z, Yu J (2013) Pt_3Co-loaded CdS and TiO_2 for photocatalytic hydrogen evolution from water. J Mater Chem A 1:12221
14. Shu D, Wang H, Wang Y, Li Y, Liu X, Chen X, Peng X, Wang X, Ruterana P, Wang H (2017) Composition dependent activity of $Fe_{1-x}Pt_x$ decorated ZnCdS nanocrystals for photocatalytic hydrogen evolution. Int J Hydrog Energy 42:20888–20894
15. Wang H, Li Y, Shu D, Chen X, Liu X, Wang X, Zhang J, Wang H (2016) $CoPt_x$-loaded $Zn_{0.5}Cd_{0.5}S$ nanocomposites for enhanced visible light photocatalytic H_2 production. Int J Energy Res 40:1280–1286
16. Wen J, Xie J, Chen X, Li X (2017) A review on g-C_3N_4-based photocatalysts. Appl Surf Sci 391:72–123
17. Han C, Lu Y, Zhang J, Ge L, Li Y, Chen C, Xin Y, Wu L, Fang S (2015) Novel PtCo alloy nanoparticle decorated 2D g-C_3N_4 nanosheets with enhanced photocatalytic activity for H_2 evolution under visible light irradiation. J Mater Chem A 3:23274–23282
18. Bi L, Gao X, Ma Z, Zhang L, Wang D, Xie T (2017) Enhanced separation efficiency of PtNix/g-C3N4 for photocatalytic hydrogen production. Chem Cat Chem 9:1–8.
19. Min S, Lu G (2012) Enhanced electron transfer from the excited Eosin Y to mpg-C_3N_4 for highly efficient hydrogen evolution under 550 nm irradiation. J Phys Chem C 116:19644–19652
20. Xu J, Li Y, Peng S, Lu G, Li S (2013) Eosin Y-sensitized graphitic carbon nitride fabricated by heating urea for visible light photocatalytic hydrogen evolution: the effect of the pyrolysis temperature of urea. Phys Chem Chem Phys 15:7657–7665
21. Yeh T, Chen S, Yeh C, Teng H (2013) Tuning the electronic structure of graphite oxide through ammonia treatment for photocatalytic generation of H_2 and O_2 from water splitting. J Phys Chem C 117:6516–6524
22. Xiang Q, Yu J (2013) Graphene-based photocatalysts for hydrogen generation. J Phys Chem Lett 4:753–759
23. Sun S, Wang W, Zhang L (2013) Bi_2WO_6 quantum dots decorated reduced graphene oxide: improved charge separation and enhanced photoconversion efficiency. J Phys Chem C 117:9113–9120
24. Li X, Yu J, Wageh S, Al-Ghamdi A, Xie J (2016) Graphene in photocatalysis: a review. Small 12:6640–6696
25. Yuan Y, Chen D, Zhong J, Yang L, Wang J, Yu Z, Zou Z (2017) Construction of a noble-metal-free photocatalytic H_2 evolution system using MoS_2/reduced graphene oxide catalyst and zinc porphyrin photosensitizer. J Phys Chem C 121:24452–24462
26. Wan W, Yu S, Dong F, Zhang Q, Zhou Y (2016) Efficient C_3N_4/graphene oxide macroscopic aerogel visible-light photocatalyst. J Mater Chem A 4:7823–7829
27. Tong Z, Yang D, Shi J, Nan Y, Sun Y, Jiang Z (2015) Three-dimensional porous aerogel constructed by g-C_3N_4 and graphene oxide nanosheets with excellent visible-light photocatalytic performance. ACS Appl Mater Interfaces 7:25693–25701
28. Liao G, Chen S, Quan X, Yu H, Zhao H (2012) Graphene oxide modified g-C_3N_4 hybrid with enhanced photocatalytic capability under visible light irradiation. J Mater Chem 22:2721–2726
29. Pu C, Wan J, Liu E, Yin Y, Li J, Ma Y, Fan J, Hu X (2017) Two-dimensional porous architecture of protonated GCN and reduced graphene oxide via electrostatic self-assembly strategy for high photocatalytic hydrogen evolution under visible light. Appl Surf Sci 399:139–150
30. Xiang Q, Yu J, Jaroniec M (2011) Preparation and enhanced visible-light photocatalytic H_2-production activity of graphene/C_3N_4 Composites. J Phys Chem C 115:7355–7363
31. Aleksandrzak M, Kukulka W, Mijowska E (2017) Graphitic carbon nitride/graphene oxide/reduced graphene oxide nanocomposites for photoluminescence and photocatalysis. Appl Surf Sci 398:56–62
32. Wang P, Guan Z, Li Q, Yang J (2018) Efficient visible-light-driven photocatalytic hydrogen production from water by using Eosin Y-sensitized novel g-C_3N_4/Pt/GO composites. J Mater Sci 53:774–786
33. Offeman W (1958) Preparation of graphitic oxide. J Am Chem Soc 80:1339
34. Han Q, Wang B, Gao J, Cheng Z, Zhao Y, Zhang Z, Qu L (2016) Atomically thin mesoporous nanomesh of graphitic C_3N_4 for high-efficiency photocatalytic hydrogen evolution. ACS Nano 10:2745–2751
35. Niu P, Zhang L, Liu G, Cheng H (2012) Graphene-like carbon nitride nanosheets for improved photocatalytic activities. Adv Funct Mater 22:4763–4770
36. Yang M, Dang Q, Xie Z, Guo H (2011) Study on CH_4 Conversion over Ce-Zr solid solution supported nano Ni-Pt bimetallic catalysts: preparation and characterization of catalysts. Mater Sci Forum 694:319–323
37. Tay Q, Kanhere P, Ng C, Chen S, Chakraborty S, Huan A, Sum T, Ahuja R, Chen Z (2015) Defect engineered g-C_3N_4 for efficient visible light photocatalytic hydrogen production. Chem Mater 27:4930–4933
38. Wang Z, Du Y, Zhang F, Zheng Z, Zhang X, Feng Q, Wang C (2013) Photocatalytic degradation of pendimethalin over Cu_2O/SnO_2/graphene and SnO_2/graphene nanocomposite photocatalysts under visible light irradiation. Mater Chem Phys 140:373–381
39. Cao S, Yuan Y, Barber J, Loo S, Xue C (2014) Noble-metal-free g-C_3N_4/$Ni(dmgH)_2$ composite for efficient photocatalytic hydrogen evolution under visible light irradiation. Appl Surf Sci 319:344–349
40. Ong W, Tan L, Chai S, Yong S (2015) Graphene oxide as a structure-directing agent for the two-dimensional interface engineering of sandwich-like graphene-g-C_3N_4 hybrid nanostructures with enhanced visible-light photoreduction of CO_2 to methane. Chem Commun (Camb) 51:858–861
41. Cao N, Yang L, Dai H, Liu T, Su J, Wu X, Luo W, Cheng G (2014) Immobilization of ultrafine bimetallic Ni-Pt nanoparticles inside the pores of metal-organic frameworks as efficient catalysts for dehydrogenation of alkaline solution of hydrazine. Inorg Chem 53:10122–10128
42. Liu Z, Lin X, Lee J, Zhang W, Han M, Gan L (2002) Preparation and characterization of platinum-based electrocatalysts on multiwalled carbon nanotubes for proton exchange membrane fuel cells. Langmuir 18:4054–4060
43. Zhen W, Gao H, Li Z, Ma J, Lu G (2016) Fabrication of low adsorption energy Ni-Mo clusters co-catalyst in metal-organic frameworks for visible photocatalytic hydrogen evolution. ACS Appl Mater Interfaces 8:10808–10819.
44. Qin L, Si G, Li X, Kang S (2013) Synergetic effect of Cu-Pt bimetallic co-catalyst on $SrTiO_3$ for efficient photocatalytic hydrogen production from water. Roy Soc Chem 00:1–3
45. Theodore L, Theresa M, Du P, Luo G, Brian L, Eisenberg R (2009) Making hydrogen from water using a homogeneous system without noble metals. J Am Chem Soc 131:9192–9194
46. Min S, Lu G (2012) Sites for high efficient photocatalytic hydrogen evolution on a limited-layered MoS_2 cocatalyst confined on graphene sheets-the role of graphene. J Phys Chem C 116:25415–25424

47. Zhang N, Shi J, Niu F, Wang J, Guo L (2015) A cocatalyst-free Eosin Y-sensitized p-type of Co_3O_4 quantum dot for highly efficient and stable visible-light-driven water reduction and hydrogen production. Phys Chem Chem Phys 17:21397–21400
48. Zhang W, Li Y, Peng S, Cai X (2014) Enhancement of photocatalytic H_2 evolution of eosin Y-sensitized reduced graphene oxide through a simple photoreaction. Beilstein J Nanotech 5:801–811